

Enhanced SARS-CoV-2 Neutralization by Secretory IgA in vitro

Zijun Wang^{1, †}, Julio C. C. Lorenzi^{1, †}, Frauke Muecksch^{2, †}, Shlomo Finklin^{1, †}, Charlotte Viant¹, Christian Gaebler¹, Melissa Cipolla¹, Hans-Heinrich Hoffman³, Thiago Y. Oliveira¹, Deena A. Oren⁴, Victor Ramos¹, Lilian Nogueira¹, Eleftherios Michailidis³, Davide F. Robbiani⁵, Anna Gazumyan¹, Charles M. Rice³, Theodora Hatziioannou², Paul D. Bieniasz^{2,6}, Marina Caskey¹, Michel C. Nussenzweig^{1,6,*}.

¹ Laboratory of Molecular Immunology, The Rockefeller University, New York, NY, USA.

² Laboratory of Retrovirology, The Rockefeller University, New York, NY, USA.

³ Laboratory of Virology and Infectious Disease, The Rockefeller University, New York, NY, USA.

⁴ Structural Biology Resource Center, The Rockefeller University, New York, NY 10065, USA

⁵ Institute for Research in Biomedicine, Università della Svizzera italiana, Bellinzona, Switzerland.

⁶ Howard Hughes Medical Institute, The Rockefeller University, New York, NY, USA.

[†] Equal contributions

* **Correspondence to:** nussen@rockefeller.edu(M.C.N)

23 **Abstract:** SARS-CoV-2 primarily infects cells at mucosal surfaces. Serum neutralizing antibody
24 responses are variable and generally low in individuals that suffer mild forms of the illness.
25 Although potent IgG antibodies can neutralize the virus, less is known about secretory antibodies
26 such as IgA that might impact the initial viral spread and transmissibility from the mucosa. Here
27 we characterize the IgA response to SARS-CoV-2 in a cohort of 149 individuals. IgA responses
28 in plasma generally correlate with IgG responses and clones of IgM, IgG and IgA producing B
29 cells that are derived from common progenitors are evident. Plasma IgA monomers are 2-fold
30 less potent than IgG equivalents. However, IgA dimers, the primary form in the nasopharynx, are
31 on average 15 times more potent than IgA monomers. Thus, secretory IgA responses may be
32 particularly valuable for protection against SARS-CoV-2 and for vaccine efficacy.

33

34 **Introduction**

35 SARS-CoV-2 encodes a trimeric spike surface protein (S) which mediates entry into host cells
36 (1, 2). The virus initially infects epithelial cells in the nasopharynx when the receptor binding
37 domain (RBD) of S interacts with angiotensin converting enzyme-2 (ACE-2) receptor (3-6).
38 SARS-CoV-2 may subsequently spread to other epithelial cells expressing ACE-2 in the lung
39 and gut. These tissues are rich in lymphoid cells that are organized into nasopharynx associated
40 and gut associated lymphoid tissues (NALT and GALT respectively). Vaccines delivered by
41 inhalation to specifically target these tissues appear to be more effective against SARS-CoV-2
42 (7). Among other specializations, NALT and GALT produce large quantities of IgA antibodies.
43 These antibodies exist as monomers in circulation where they make up 15% of the serum
44 antibody pool. However, IgA is found in higher concentrations in secretions where it exists
45 predominantly as a dimer covalently linked by J chain (8-10).

46

47 Although most individuals produce antibodies in response to SARS-CoV-2 infection, the
48 neutralizing response is highly variable with as many as 30% of the population showing levels of
49 neutralizing activity below 1:50 in pseudovirus assays (11, 12). Neutralization is associated with
50 prolonged infection and RBD binding activity as measured by ELISA (11-13). IgG antibody
51 cloning experiments from recovered individuals have revealed that neutralizing antibodies target
52 several distinct non-overlapping epitopes on the RBD (11, 14-18). Some of these antibodies are
53 potently neutralizing and can prevent or treat infection in animal models (15-19).

54

55 Consistent with the fact that SARS CoV-2 initially infects in the nasopharynx, IgA antibodies
56 that bind to SARS-CoV-2 are produced rapidly after infection and remain elevated in the plasma
57 for at least 40 days after the onset of symptoms (20-23). IgA antibodies bind to the RBD and can
58 neutralize SARS-CoV-2 (20-22). However, the precise contribution and molecular nature of the
59 IgA response to SARS-CoV-2 has not been reported to date. Here we examine a cohort of 149
60 convalescent individuals with measurable plasma neutralizing activity for the contribution of IgA
61 to anti-SARS-CoV-2 antibody responses. Cloning IgA antibodies from single B cells reveals that
62 the neutralizing activity of monomeric IgA is generally lower than corresponding IgGs but
63 dimeric IgAs are on average 15-fold more potent than their monomeric counterparts.

64

65 **Results**

66 **Plasma anti-SARS-CoV-2 RBD IgA**

67 IgM, IgG and IgA account for 5%, 80% and 15% of the antibodies in plasma, respectively. IgG
68 responses to RBD are strongly correlated with neutralizing activity (11, 13-17, 24-28). To

69 examine the contribution of IgA to the anti-SARS-CoV-2 RBD response we tested plasma
70 samples for binding to the RBD by a validated ELISA. A positive control sample (COV-21) was
71 included for normalization of the area under the curve (AUC) and 8 independent healthy donor
72 samples were included as negative controls (Fig. 1A, (11)). Whereas 78% and 15% of the
73 individuals in this cohort showed IgG and IgM anti-RBD levels that were at least 2 standard
74 deviations above control, only 33% did so for IgA (Fig. 1A and B, (11)). Thus, in individuals
75 studied on average 40 days after infection the circulating levels of anti-RBD IgA is more modest
76 than IgG and higher than IgM.

77
78 Anti-RBD IgA titers were correlated with duration and severity of symptoms but not timing of
79 sample collection relative to onset (Fig. 1C, and fig.S1A, B). Similar to IgG, females had lower
80 levels of IgA than males and hospitalized individuals showed higher anti-RBD IgA titers than
81 those with milder symptoms, but there was no correlation with age (Fig. 1D and E, fig. S1C). Of
82 note, individuals that suffered gastrointestinal symptoms showed significantly higher plasma
83 anti-RBD IgA but not IgG titers (Fig. 1F and fig. S1D).

84

85 **Neutralization activity of purified IgG and IgA**

86 To compare the neutralizing activity of plasma IgA to IgG directly we purified the 2 isotypes
87 from the plasma of all 99 individuals in our cohort that showed measurable plasma neutralizing
88 activity and tested the two isotypes in HIV-1 based SARS-CoV-2 pseudovirus neutralization
89 assays (11). The activity of both isotypes was directly correlated with anti-RBD binding titers
90 and overall plasma neutralizing activity (Fig. 2A-D). In addition, there was good correlation
91 between the neutralizing activity of IgG and IgA in a given individual (Fig. 2E). However,

92 potency of each of the 2 isotypes varied by as much as 2 orders of magnitude between
93 individuals (Fig. 2F). Purified IgG was generally more potent than IgA in neutralizing SARS-
94 CoV-2 pseudovirus *in vitro*. The geometric mean IC₅₀ for IgG was 384 nM vs. 709 nM for IgA
95 ($P < 0.0001$, Fig. 2F). Nevertheless, IgAs were more potent than IgGs in 25% of the individuals
96 tested (fig. S2A). The 2 isotypes also differed in that the overall potency of purified IgG was
97 correlated with symptom severity and was higher in hospitalized individuals, but purified IgA
98 was not (Fig. 2G and fig. S2B- D). Finally, the potency of the purified IgA was greater in
99 individuals that suffered from gastrointestinal symptoms, but IgG was not (Fig. 2H and fig. S2E).

100

101 **Monoclonal anti-SARS-CoV-2 IgM and IgA antibodies**

102 To determine the nature of the IgM and IgA anti-RBD antibodies elicited by SARS-CoV-2
103 infection we used flow cytometry to purify single B lymphocytes that bind to RBD and cloned
104 their antibodies. We obtained 109 IgM and 74 IgA (64 IgA1 and 10 IgA2) matched Ig heavy and
105 light chain sequences by reverse transcription and subsequent isotype specific PCR from 3
106 convalescent individuals (Fig. 3A, B). As reported for IgG antibodies (11, 14, 17, 26, 29), the
107 overall number of mutations was generally low when compared to antibodies obtained from
108 individuals suffering from chronic infections such as Hepatitis-B or HIV-1 (30, 31) (fig. S3A,
109 B). However, the number of V gene nucleotide mutations in IgM and IgA heavy and light chains
110 varied between individuals. For example, in donor COV21 the number of IgM and IgA heavy
111 chain mutations was similar. In contrast, IgM heavy and light chain nucleotide mutations were
112 significantly greater than IgA mutations in COV47 (fig. S3B). CDR3 length was significantly
113 shorter for IgM than IgA and IgG antibodies and hydrophobicity was slightly higher for IgM
114 over control but not for IgA and IgG (figs. S4 and S5). Compared to the normal human antibody

115 repertoire, several IgA and IgM VH genes were over-represented including VH3-53 which can
116 make key contacts with the RBD through germline encoded CDRH1 and CDRH2 (11, 32, 33)
117 (fig. S6).

118
119 Like IgG antibodies (11) IgA and IgM antibodies were found in expanded clones in all 3 of the
120 individuals examined. Overall 66.2% and 66.1% of all the IgA and IgM sequences examined
121 were members of expanded clones (Fig. 3A, B and table S1). Nearly identical sequences were
122 shared among the 3 isotypes in clones found in all 3 individuals indicating that switch
123 recombination occurred during B cell clonal expansion in response to SARS-CoV-2 (Fig.3B). In
124 total 11 out of 55 antigen-specific B cell clones in circulation belonged to expanded clones that
125 contained members expressing different constant regions (Fig. 3C and tables S1 and S2). When
126 compared directly, the neutralizing activity of antibodies that were members of B cell clones
127 producing IgA or IgG varied and did not correlate with one or the other isotype (table S3).

128
129 To examine the binding properties of the anti-SARS-CoV-2 monoclonals we expressed 46 IgMs
130 and 35 IgAs (table S4). IgM variable regions were produced on an IgG1 backbone to facilitate
131 expression and purification. IgAs were expressed as native IgA1 or IgA2 monomers. ELISA
132 assays on RBD showed that 100% and 91.3% of the IgA and IgM antibodies bound to the RBD
133 with an average half-maximal effective concentration of 52.8 ng/ml and 101.6 ng/ml respectively
134 (fig. S7A and table S5).

135
136 To determine neutralizing activity of the IgM and IgA antibodies we tested them against an HIV-
137 1 based SARS-CoV-2 pseudovirus as IgGs and native IgA monomers respectively. Among the

138 42 RBD binding IgM antibodies tested we found 10 that neutralized the virus in the ng/ml range
139 with geometric mean half-maximal inhibitory concentrations (IC_{50}) of 114.0 nanograms per
140 milliliter (Fig. 4A and fig. S7B, table S5). In contrast, 32 out of 35 RBD binding IgA antibodies
141 tested neutralized the virus in the ng/ml range with geometric mean half-maximal inhibitory
142 concentrations (IC_{50}) of 53.6 nanograms per milliliter (Fig. 4A and fig. S7B, table S5). Thus,
143 IgM antibodies expressed as monomeric IgGs show lower neutralizing activity than either native
144 IgA or IgG monomers (Fig. 4A).

145

146 **Dimeric anti- SARS-CoV-2 IgA is more potent than monomeric IgA**

147 To determine whether these IgAs targeted the same epitopes as previously characterized IgGs we
148 performed bilayer interferometry experiments in which a preformed antibody-RBD complex
149 consisting of C144-RBD, or C121-RBD or C135-RBD or CR3022-RBD (Fig. 4B) was exposed
150 to a monomeric IgA monoclonal. C144 and C121 recognize the ACE-2 interaction domain of the
151 RBD, C135 and CR3022 neutralize without interfering with ACE-2 binding (Fig. 4C) (11, 32,
152 34). Two of the IgA's were in the C144 category, 5 were similar to C121, and 2 resembled C135
153 (Fig. 4C and fig. S9). Thus, RBD recognition by neutralizing IgA is similar to IgG.

154

155 Mucosal IgA exists predominantly as a dimer. To examine the neutralizing activity of IgA
156 dimers we co-expressed 8 IgA1s and 1 IgA2 with J chain to produce mixtures of monomers and
157 dimers that were purified by size exclusion chromatography (fig. S8). When compared in
158 pseudovirus neutralization assays, 8 out of 9 IgA dimers were more potent than the
159 corresponding monomers with differences in activity ranging from 3.8 to 113-fold (Fig. 4D, fig.
160 S10A and table S6). The relative increase in neutralizing activity between monomer and dimer

161 was inversely correlated with the neutralizing activity of the monomer in this assay (fig. S10B.
162 IC_{50} : $r=0.80$, $P=0.014$). For example, whereas C437, the most potent antibody, showed
163 equivalent activity as a monomer and dimer, C408, one of the least potent antibodies, was 113-
164 fold more potent as a dimer (fig. S10B).

165
166 IgA monomers and dimers were also compared in SARS-CoV-2 microneutralization assays.
167 Neutralizing activities of the 9 monomers and 9 dimers correlated strongly with those measured
168 in the pseudovirus neutralization assay (fig. S10C. IC_{50} : $r=0.84$, $P<0.0001$; IC_{90} : $r=0.91$,
169 $P<0.0001$). On average, there was a 15-fold geometric mean increase in activity for the dimer
170 over the monomer against SARS-CoV-2 and less variability in the degree of enhancement in
171 microneutralization compared to pseudovirus assays (Fig. 4D, fig. S10D and E, and table S6).
172 Thus, dimeric IgA is far more potent than monomeric IgA against SARS-CoV-2 (Fig. 4D).

173

174 **Discussion**

175 Neutralizing antibody titers are the best correlates of protection in most vaccines (35). Among
176 antibody isotypes, secretory IgA which is found at mucosal surfaces, plays a crucial role in
177 protecting against pathogens that target these surfaces (36). We find that serum IgA responses to
178 SARS-CoV-2 correlate with IgG responses. Although the monomeric form of IgA found in
179 serum is on average 2-fold less potent than IgG, the dimeric secretory form of IgA found in
180 mucosa is over one log more potent than the monomer against authentic SARS-CoV-2 which
181 makes it a far more potent neutralizer than IgG.

182

183 The increased potency of the dimeric form of IgA suggests that crosslinking the S protein on the
184 viral surface enhances neutralizing activity either directly or simply through increased apparent
185 affinity. This observation is consistent with the finding that monovalent Fab fragments of serum
186 IgG antibodies are far less potent than the intact antibody (32). Whether this effect is due to
187 inter- or intra-spike crosslinking is not known, but it indicates that antibodies or drugs designed
188 to block entry by binding to the RBD could be made more potent by increasing their valency.

189

190 A number of different candidate vaccines to SARS-CoV-2 are currently being evaluated in the
191 clinic. Secretory IgA responses may be particularly important to these efforts in that potent
192 dimeric forms of these antibodies are found at the mucosal surfaces where cells are initially
193 targeted by SARS-CoV-2. Thus, even vaccines that elicit modest neutralizing activity in serum
194 may be protective because the secretory polymeric forms of antibodies in mucosa can neutralize
195 the virus. Vaccines that are specifically designed to elicit mucosal IgA responses may be
196 particularly effective preventing SARS-CoV-2 infection (7).

197

198 **Reference and notes**

- 199 1. A. C. Walls *et al.*, Structure, Function, and Antigenicity of the SARS-CoV-2 Spike
200 Glycoprotein. *Cell* **181**, 281-292 e286 (2020).
- 201 2. P. Zhou *et al.*, A pneumonia outbreak associated with a new coronavirus of probable bat
202 origin. *Nature* **579**, 270-273 (2020).
- 203 3. M. Hoffmann *et al.*, SARS-CoV-2 Cell Entry Depends on ACE2 and TMPRSS2 and Is
204 Blocked by a Clinically Proven Protease Inhibitor. *Cell* **181**, 271-280 e278 (2020).

- 205 4. R. Lu *et al.*, Genomic characterisation and epidemiology of 2019 novel coronavirus:
206 implications for virus origins and receptor binding. *Lancet* **395**, 565-574 (2020).
- 207 5. D. Wrapp *et al.*, Cryo-EM structure of the 2019-nCoV spike in the prefusion
208 conformation. *Science* **367**, 1260-1263 (2020).
- 209 6. J. Lan *et al.*, Structure of the SARS-CoV-2 spike receptor-binding domain bound to the
210 ACE2 receptor. *Nature* **581**, 215-220 (2020).
- 211 7. A. O. Hassan *et al.*, A single-dose intranasal ChAd vaccine protects upper and lower
212 respiratory tracts against SARS-CoV-2. *Cell*, (2020).
- 213 8. B. J. Underdown, J. M. Schiff, Immunoglobulin A: strategic defense initiative at the
214 mucosal surface. *Annu Rev Immunol* **4**, 389-417 (1986).
- 215 9. M. E. Koshland, The coming of age of the immunoglobulin J chain. *Annu Rev Immunol*
216 **3**, 425-453 (1985).
- 217 10. O. Pabst, New concepts in the generation and functions of IgA. *Nat Rev Immunol* **12**,
218 821-832 (2012).
- 219 11. D. F. Robbiani *et al.*, Convergent antibody responses to SARS-CoV-2 in convalescent
220 individuals. *Nature*, (2020).
- 221 12. F. Wu *et al.*, Evaluating the Association of Clinical Characteristics With Neutralizing
222 Antibody Levels in Patients Who Have Recovered From Mild COVID-19 in Shanghai,
223 China. *JAMA Intern Med*, (2020).
- 224 13. B. Ju *et al.*, Human neutralizing antibodies elicited by SARS-CoV-2 infection. *Nature*,
225 (2020).
- 226 14. P. J. M. Brouwer *et al.*, Potent neutralizing antibodies from COVID-19 patients define
227 multiple targets of vulnerability. *Science*, (2020).

- 228 15. L. Liu *et al.*, Potent neutralizing antibodies directed to multiple epitopes on SARS-CoV-2
229 spike. *Nature*, (2020).
- 230 16. Y. Wu *et al.*, A noncompeting pair of human neutralizing antibodies block COVID-19
231 virus binding to its receptor ACE2. *Science* **368**, 1274-1278 (2020).
- 232 17. T. F. Rogers *et al.*, Isolation of potent SARS-CoV-2 neutralizing antibodies and
233 protection from disease in a small animal model. *Science*, (2020).
- 234 18. S. J. Zost *et al.*, Potently neutralizing and protective human antibodies against SARS-
235 CoV-2. *Nature*, (2020).
- 236 19. A. Baum *et al.*, REGN-COV2 antibody cocktail prevents and treats SARS-CoV-2
237 infection in rhesus macaques and hamsters. *bioRxiv*, 2020.2008.2002.233320 (2020).
- 238 20. H. Ma *et al.*, Serum IgA, IgM, and IgG responses in COVID-19. *Cell Mol Immunol* **17**,
239 773-775 (2020).
- 240 21. D. Sterlin *et al.*, IgA dominates the early neutralizing antibody response to SARS-CoV-2.
241 *medRxiv*, 2020.2006.2010.20126532 (2020).
- 242 22. H. Q. Yu *et al.*, Distinct features of SARS-CoV-2-specific IgA response in COVID-19
243 patients. *Eur Respir J*, (2020).
- 244 23. J. Seow *et al.*, Longitudinal evaluation and decline of antibody responses in SARS-CoV-
245 2 infection. *medRxiv*, 2020.2007.2009.20148429 (2020).
- 246 24. X. Chi *et al.*, A neutralizing human antibody binds to the N-terminal domain of the Spike
247 protein of SARS-CoV-2. *Science*, (2020).
- 248 25. Y. Cao *et al.*, Potent Neutralizing Antibodies against SARS-CoV-2 Identified by High-
249 Throughput Single-Cell Sequencing of Convalescent Patients' B Cells. *Cell* **182**, 73-84
250 e16 (2020).

- 251 26. C. Kreer *et al.*, Longitudinal Isolation of Potent Near-Germline SARS-CoV-2-
252 Neutralizing Antibodies from COVID-19 Patients. *Cell*, (2020).
- 253 27. F. Schmidt *et al.*, Measuring SARS-CoV-2 neutralizing antibody activity using
254 pseudotyped and chimeric viruses. *J Exp Med* **217**, (2020).
- 255 28. R. Shi *et al.*, A human neutralizing antibody targets the receptor-binding site of SARS-
256 CoV-2. *Nature*, (2020).
- 257 29. E. Seydoux *et al.*, Analysis of a SARS-CoV-2-Infected Individual Reveals Development
258 of Potent Neutralizing Antibodies with Limited Somatic Mutation. *Immunity* **53**, 98-105
259 e105 (2020).
- 260 30. J. F. Scheid *et al.*, Broad diversity of neutralizing antibodies isolated from memory B
261 cells in HIV-infected individuals. *Nature* **458**, 636-640 (2009).
- 262 31. Q. Wang *et al.*, A Combination of Human Broadly Neutralizing Antibodies against
263 Hepatitis B Virus HBsAg with Distinct Epitopes Suppresses Escape Mutations. *Cell Host*
264 *Microbe*, (2020).
- 265 32. C. O. Barnes *et al.*, Structures of Human Antibodies Bound to SARS-CoV-2 Spike
266 Reveal Common Epitopes and Recurrent Features of Antibodies. *Cell*, (2020).
- 267 33. M. Yuan *et al.*, Structural basis of a shared antibody response to SARS-CoV-2. *Science*,
268 (2020).
- 269 34. M. Yuan *et al.*, A highly conserved cryptic epitope in the receptor binding domains of
270 SARS-CoV-2 and SARS-CoV. *Science* **368**, 630-633 (2020).
- 271 35. S. A. Plotkin, Correlates of protection induced by vaccination. *Clin Vaccine Immunol* **17**,
272 1055-1065 (2010).

- 273 36. K. Chen, G. Magri, E. K. Grasset, A. Cerutti, Rethinking mucosal antibody responses:
274 IgM, IgG and IgD join IgA. *Nat Rev Immunol* **20**, 427-441 (2020).
- 275 37. A. Grifoni *et al.*, Targets of T Cell Responses to SARS-CoV-2 Coronavirus in Humans
276 with COVID-19 Disease and Unexposed Individuals. *Cell* **181**, 1489-1501 e1415 (2020).
- 277 38. F. Amanat *et al.*, A serological assay to detect SARS-CoV-2 seroconversion in humans.
278 *Nat Med* **26**, 1033-1036 (2020).
- 279 39. T. Tiller *et al.*, Efficient generation of monoclonal antibodies from single human B cells
280 by single cell RT-PCR and expression vector cloning. *J Immunol Methods* **329**, 112-124
281 (2008).
- 282 40. L. von Boehmer *et al.*, Sequencing and cloning of antigen-specific antibodies from
283 mouse memory B cells. *Nat Protoc* **11**, 1908-1923 (2016).
- 284 41. D. F. Robbiani *et al.*, Recurrent Potent Human Neutralizing Antibodies to Zika Virus in
285 Brazil and Mexico. *Cell* **169**, 597-609 e511 (2017).
- 286 42. J. Ye, N. Ma, T. L. Madden, J. M. Ostell, IgBLAST: an immunoglobulin variable domain
287 sequence analysis tool. *Nucleic Acids Res* **41**, W34-40 (2013).
- 288 43. N. T. Gupta *et al.*, Change-O: a toolkit for analyzing large-scale B cell immunoglobulin
289 repertoire sequencing data. *Bioinformatics* **31**, 3356-3358 (2015).
- 290 44. C. Soto *et al.*, High frequency of shared clonotypes in human B cell receptor repertoires.
291 *Nature* **566**, 398-402 (2019).
- 292 45. Y. Guo, K. Chen, P. D. Kwong, L. Shapiro, Z. Sheng, cAb-Rep: A Database of Curated
293 Antibody Repertoires for Exploring Antibody Diversity and Predicting Antibody
294 Prevalence. *Front Immunol* **10**, 2365 (2019).
- 295

296 **Acknowledgements:** We thank all study participants who devoted time to our research; Drs.
297 Barry Coller and Sarah Schlesinger, the Rockefeller University Hospital Clinical Research
298 Support Office and nursing staff; Ivo Lorenz and the Tri-I TDI antibody team for help with BLI
299 measurements. All members of the M.C.N. laboratory for helpful discussions, Maša Jankovic for
300 laboratory support. **Funding:** This work was supported by NIH grant P01-AI138398-S1 and 2U1
301 9AI111825 to M.C.N. and C.M.R.; George Mason University Fast Grants to D.F.R. and C.M.R.,
302 3 R01-AI091707-10S1 to C.M.R.; The G. Harold and Leila Y. Mathers Charitable Foundation to
303 C.M.R.; European ATAC consortium (EC 101003650) to D.F.R. C.G. was supported by the
304 Robert S. Wennett Post-Doctoral Fellowship, in part by the National Center for Advancing
305 Translational Sciences (National Institutes of Health Clinical and Translational Science Award
306 programme, grant UL1 TR001866) and by the Shapiro-Silverberg Fund for the Advancement of
307 Translational Research. P.D.B. and M.C.N. are Howard Hughes Medical Institute Investigators.
308 **Author contributions:** Z.W., J.C.C.L., F.M., S.F. and M.C.N. conceived, designed and analyzed
309 the experiments. Z.W., J.C.C.L., F.M., S.F., C.V., M.C., H.-H.H. L.N. and E.M. carried out all
310 experiments. D.F.R., M. Caskey and C.G. designed clinical protocols. M.C., A.G. and D.O.
311 produced antibodies. T.Y.O., and V.R. performed bioinformatic analysis. C.M.R., T.M. and
312 P.D.B. helped designing the experiments. Z.W., J.C.C.L., F.M., S.F. and M.C.N. wrote the
313 manuscript with input from all co-authors. **Declaration of conflict:** In connection with this work
314 The Rockefeller University has filed a provisional patent application on which D.F.R. and
315 M.C.N. are inventors. **Data and materials availability:** Data are provided in table S1, 2 ,4. The
316 raw sequencing data associated with Fig. 3 has been deposited at Github
317 (<https://github.com/stratust/igpipeline>). This study uses data from a database of human shared
318 BCR clonotypes "<https://cabrep.c2b2.columbia.edu/home/>", and from 'cAb-Rep: A Database of

319 Curated Antibody Repertoires for Exploring Antibody Diversity and Predicting Antibody
320 Prevalence' and 'High frequency of shared clonotypes in human B cell receptor repertoires'.
321 Computer code to process the antibody sequences are available at GitHub
322 (<https://github.com/stratust/igpipeline>).

323
324 **Supplementary materials:**

325 Materials and Methods

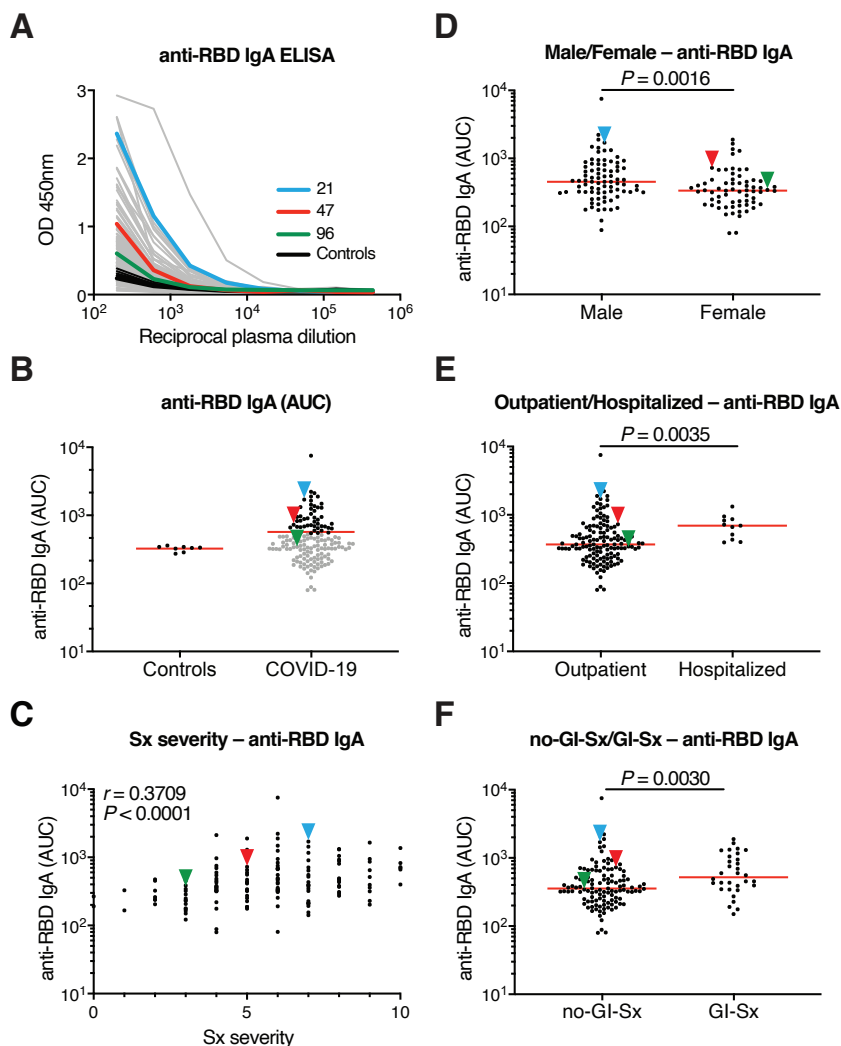
326 Figs. S1 to S10

327 Tables S1 to S7

328 Reference (37-45)

329

330

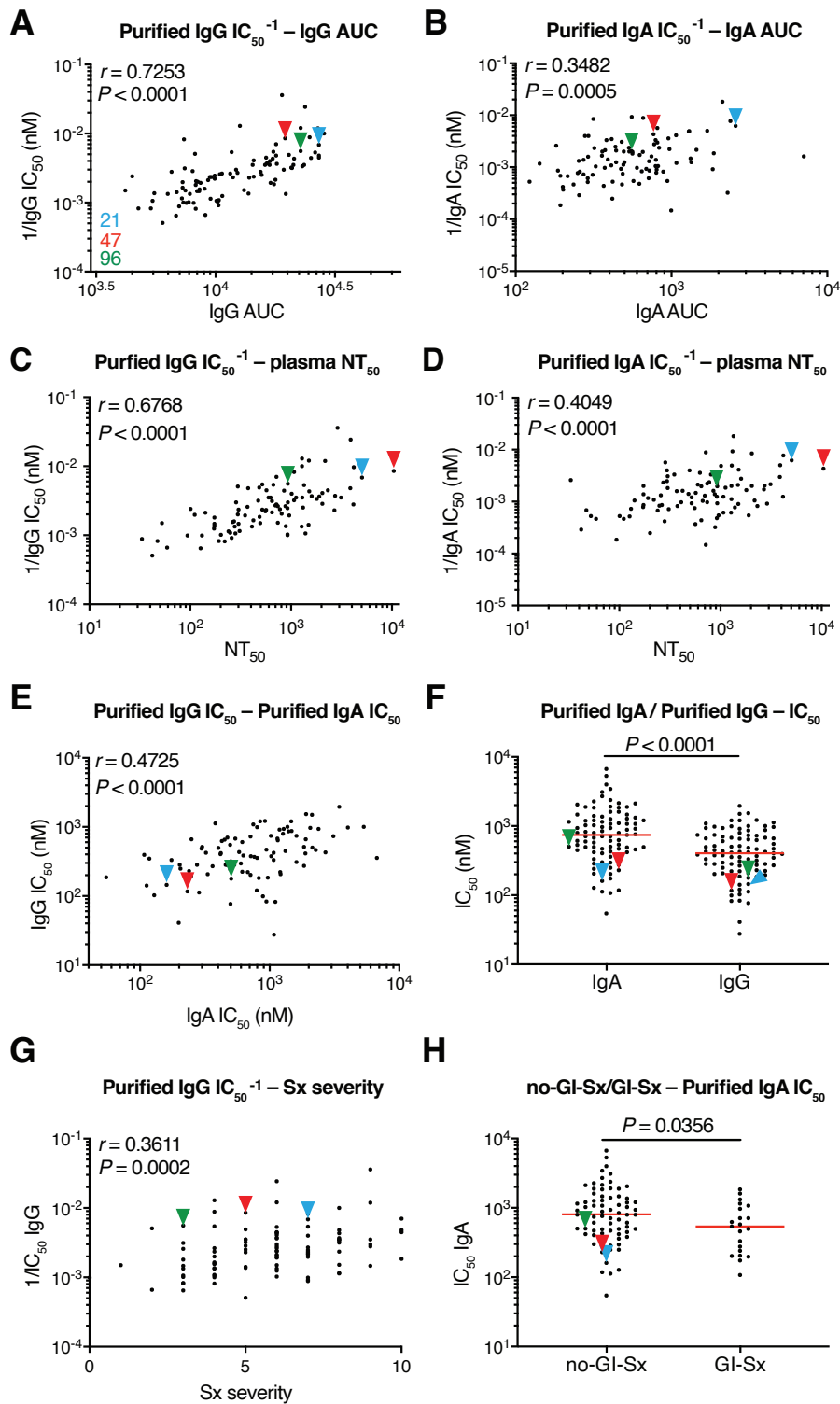


331
332

Fig. 1 Plasma IgA against SARS-CoV-2 RBD. (A) ELISAs measuring plasma IgA reactivity to RBD. Graph shows optical density units at 450 nm (OD, Y axis) and reciprocal plasma dilutions (X axis). Negative controls in black; individuals 21, 47, 96 in blue, red and green lines and arrowheads, respectively (11). (B) Graph shows normalized area under the curve (AUC) for 8 controls and each of 149 individuals in the cohort. Horizontal bar indicates mean values. Black dots indicate the individuals that are 2 STDV over the mean of controls. (C) Subjective Symptom (Sx) severity (X axis) is plotted against the normalized AUC for IgA binding to RBD (Y axis). r

333
334
335
336
337
338

339 = 0.3709, $P < 0.0001$. (D) Normalized AUC of anti-RBD IgA ELISA for males (n=83) and
340 females (n=66); $P = 0.0016$. (E) Normalized AUC of anti-RBD IgA ELISA for outpatients
341 (n=138) and hospitalized (n=11) individuals; $P = 0.0035$. (F) Normalized AUC of anti-RBD IgA
342 ELISA for patients with gastrointestinal (GI) symptoms (n=32) and without GI symptoms
343 (n=117); $P = 0.0030$. The r and P values for the correlations in (C) were determined by two-
344 tailed Spearman's. For (D-F) horizontal bars indicate median values. Statistical significance was
345 determined using two-tailed Mann-Whitney U test.
346



347

348

Fig. 2 SARS-CoV-2 pseudovirus neutralization by purified IgA and IgG. Neutralization

349

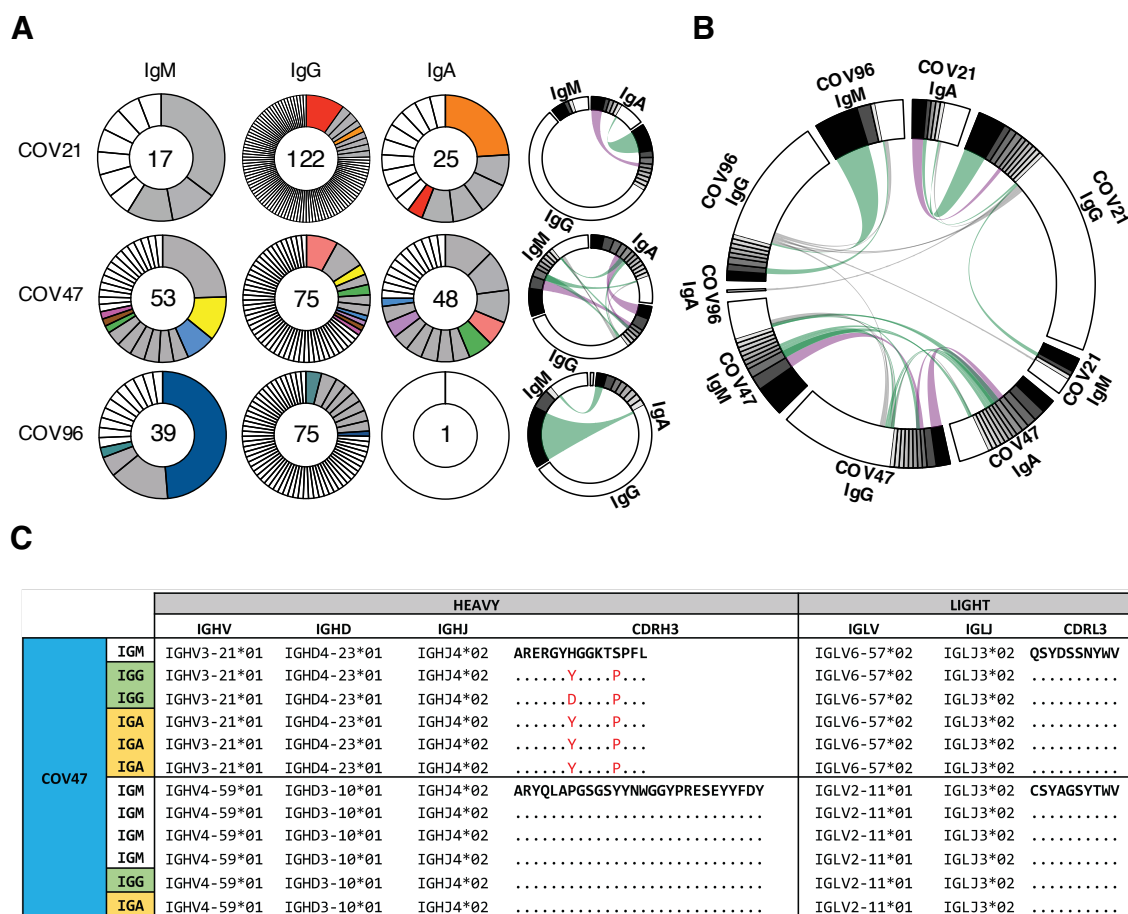
activity of plasma-purified IgG and IgA from 99 participants measured in cell lysates of

350 HT1080_{ACE2}cl.14 cells 48 h after infection with nanoluc-expressing SARS-CoV-2 pseudovirus.
351 (A) Normalized AUC for plasma IgG anti-RBD ELISA (X axis) plotted against purified IgG
352 pseudovirus neutralization 1/IC₅₀ values (Y axis). $r = 0.7253$, $P < 0.0001$. (B) Normalized AUC
353 for plasma IgA ELISA (X axis) plotted against purified IgA pseudovirus neutralization 1/IC₅₀
354 values (Y axis). $r = 0.3482$, $P = 0.0005$. (C) Published plasma NT₅₀ values (*II*) (X axis) plotted
355 against purified IgG pseudovirus neutralization 1/IC₅₀ values (Y axis). $r = 0.6768$, $P <$
356 0.0001 . (D) Published plasma NT₅₀ values (*II*) (X axis) plotted against purified IgA pseudovirus
357 neutralization 1/IC₅₀ values (Y axis). $r = 0.4049$, $P < 0.0001$. (E) Purified IgA pseudovirus
358 neutralization IC₅₀ values (X axis) plotted against purified IgG pseudovirus neutralization IC₅₀
359 values. $r = 0.4725$, $P < 0.0001$. (F) Comparison of purified IgA and IgG pseudovirus
360 neutralization IC₅₀ values, $P < 0.0001$. (G) Symptom severity plotted against purified IgG
361 pseudovirus neutralization 1/IC₅₀ values. $r = 0.3611$, $P = 0.0002$. (H) Purified IgA pseudovirus
362 neutralization IC₅₀ values for patients with GI symptoms (n=21) and without GI symptoms
363 (n=74); $P = 0.0356$. The r and p values in (A-E, G) were determined by two-tailed Spearman's
364 correlations. In (F and H), p values were determined by two-tailed Mann–Whitney U-tests and
365 horizontal bars indicate median values.

366

367

368



369

370

371

372

373

374

375

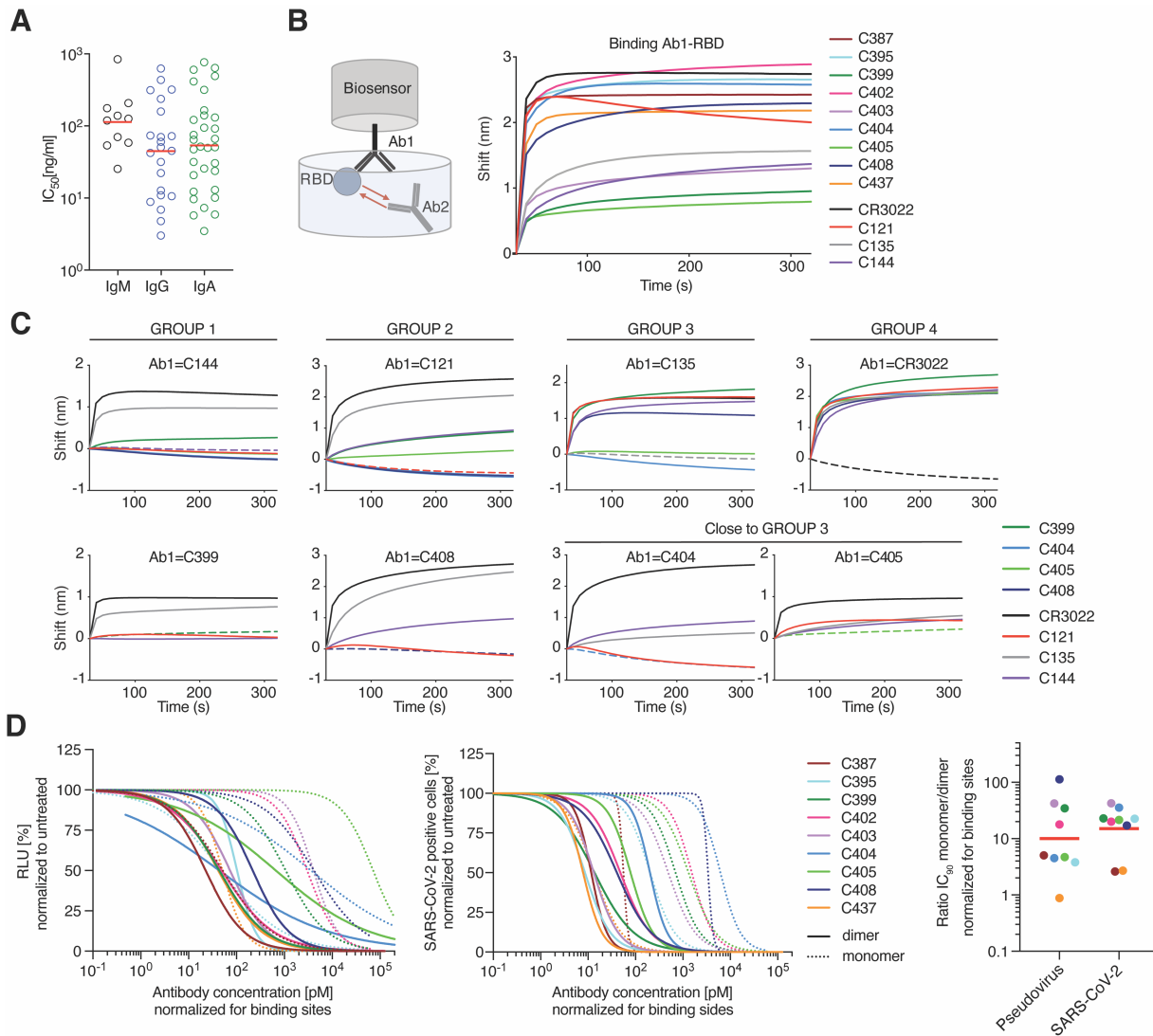
376

377

Fig. 3 Monoclonal anti-SARS-CoV-2 RBD IgM, IgG and IgA. (A) Clonal expansion of B cells producing of IgM, IgG and IgA from three individuals. The number in the inner circle indicates the number of sequences analyzed for the individual denoted above the circle. Pie slices size is proportional to the number of clonally related sequences. Colored pie slices indicate clones or singlets that share the same IGHV and IGLV genes, and highly similar CDR3s. Grey indicates clones that are not shared. White indicates singlets that are not shared. The right side circos plots show the relationship between antibodies of different isotypes that share same IGH V(D)J and IGL VJ genes, and highly similar CDR3s. Purple, green and grey lines connect related

378 clones, clones and singles, and singles to each other, respectively. (B) Circos plot shows
379 sequences from all 3 individuals with clonal relationships depicted as in (A). (C) Sample
380 sequence alignment for antibodies of different isotypes that display same IGH V(D)J and IGL VJ
381 genes and highly similar CDR3s. Amino acid differences in CDR3s to the reference sequence
382 (bold) are indicated in red, dashes indicate missing amino acids and dots represent identical
383 amino acids.
384

385



386

387 **Fig. 4 IgA dimers neutralize SARS-CoV-2 more potently than monomers.** (A) Pseudovirus
 388 IC₅₀ neutralization values for IgA, and IgM monoclonals and published IgG monoclonals from
 389 the same individuals (11). Antibodies with IC₅₀ less than 1000 ng/ml are shown. Red lines
 390 indicate geometric mean. (B) Diagrammatic representation of biolayer interferometry experiment
 391 (left panel). Binding of C387, C395, C399, C402, C403, C404, C405, C408, C437, CR3022,
 392 C121, C135, C144 to RBD (right panel). (C) Second antibody (Ab2) binding to preformed first
 393 antibody (Ab1)-RBD complexes. Dotted line denotes when Ab1 and Ab2 are the same, and Ab2

394 is according to the colour-coding in g, h, i, Group 1 antibodies were tested. (D) The normalized
395 relative luminescence values for cell lysates of 293T_{ACE2} cells after infection with SARS-CoV-2
396 pseudovirus (left panel) or normalized percentage of SARS-CoV-2 positive VeroE6 cells 48 h
397 after infection with SARS-CoV-2 authentic virus (middle panel; values obtained in the absence
398 of antibody are plotted at $x=0.1$ to be visible on log-scale) in the presence of increasing
399 concentrations of monoclonal antibodies C387, C395, C399, C402, C403, C404, C405, C408,
400 C437 as monomers or dimers. Shown are four-parameter nonlinear regression curve fits of
401 normalized data. Comparison of the ratio of IC₉₀ values of monomer to dimers, normalized to
402 number of antibody binding sites (right panel).

403

404 **Materials and Methods**

405 **Human Study participants**

406 Samples were obtained from 149 individuals under a study protocol approved by the Rockefeller University in New
407 York from April 1 through May 8, 2020 as described in (11). All participants provided written informed consent
408 before participation in the study and the study was conducted in accordance with Good Clinical Practice and clinical
409 data collection. The study was performed in compliance with all relevant ethical regulations and the protocol was
410 approved by the Institutional Review Board (IRB) of the Rockefeller University.

411

412 **Purification and quantification of IgA and IgG from plasma**

413 IgA and IgG were purified from samples with measurable neutralizing activity, against SARS-CoV-2-RBD (11).
414 300µl of plasma was diluted with PBS heat-inactivated (56°C for 1 hr) and incubated with peptide M/Agarose
415 (Invivogen) or Protein G/Agarose (GE lifeSciences) overnight at 4 °C. The suspension was transferred to
416 chromatography columns and washed with 10 column volumes of 1X-PBS. IgA and IgG were then eluted with
417 1.5ml of 0.1M glycine (pH=3.0) and pH was immediately adjusted to 7.5 with 1M Tris (pH=8.0). 1X-PBS buffer
418 exchange was achieved using Amicon® Ultra centrifugal filters (Merck Millipore) through a 30-kD membrane
419 according to the manufacturer's instructions. IgA and IgG concentrations were determined by measurement of
420 absorbance at 280nm using a NanoDrop (Thermo Scientific) instrument and samples were stored at 4°C.

421

422 **ELISAs**

423 ELISAs to evaluate the IgG or IgA binding to SARS-CoV-2 RBD were performed as previously described using a
424 validated assay (37, 38). High binding 96 half well plates (Corning #3690) were coated with 50 µL per well of a
425 1µg/mL protein solution in PBS overnight at 4 °C. Plates were washed 6 times with washing buffer (1xPBS with
426 0.05% Tween 20 (Sigma-Aldrich)) and incubated with 170 µL blocking buffer per well (1xPBS with 2% BSA and
427 0.05% Tween20 (Sigma) for 1 hour at room temperature (RT). Immediately after blocking, monoclonal antibodies
428 or plasma samples were added in PBS and incubated for 1 hr at RT. Plasma samples were assayed at a 1:200 starting
429 dilution and seven additional 3-fold serial dilutions. Monoclonal antibodies were tested at 10 µg/ml starting
430 concentration and 10 additional 4-fold serial dilutions. Plates were washed 6 times with washing buffer and then
431 incubated with anti-human IgG (Jackson Immuno Research 109-036-088) or anti-human IgA (Sigma A0295)

432 secondary antibody conjugated to horseradish peroxidase (HRP) in blocking buffer at 1:5000 or 1:3000 dilution
433 respectively. Plates were developed by addition of the HRP substrate, TMB (ThermoFisher) for 10 minutes (plasma
434 samples) or 4 minutes (monoclonal antibodies), then the developing reaction was stopped by adding 50µl 1M
435 H₂SO₄. ODs were measured at 450 nm in a microplate reader (FluoStar Omega, BMG Labtech). For plasma
436 samples, a positive control (plasma from patient COV21, diluted 200-fold in PBS) and negative control historical
437 plasma samples was added in duplicate to every assay plate for validation. The average of its signal was used for
438 normalization of all the other values on the same plate with Excel software prior to calculating the area under the
439 curve using Prism 8 (GraphPad).

440

441 **Cell lines**

442 HT1080_{Ace2} cl.14 cells (27), 293T_{Ace2} cells (11) and VeroE6 kidney epithelial cells were cultured in Dulbecco's
443 modified Eagle medium (DMEM) supplemented with 10% FCS at 37 °C and 5% CO₂. In addition, medium for
444 Ace2-overexpressing cell lines contained 5 µg/ml blasticidin and medium for VeroE6 cells was supplemented with 1
445 % nonessential amino acids. All cell lines have been tested negative for contamination with mycoplasma and
446 parental cell lines were obtained from the ATCC.

447

448 **Pseudotyped virus neutralization assay**

449 SARS-CoV-2 pseudotyped particles were produced by co-transfection of pSARS-CoV-2 S_{trunc} and pNL4-3ΔEnv-
450 nanoluc in 293T cells (11, 27). Four-fold serially diluted purified plasma IgG/IgA from COVID-19 convalescent
451 individuals and healthy donors or monoclonal antibodies were incubated with the SARS-CoV-2 pseudotyped virus
452 for 1 hour at 37 °C. Subsequently, the mixture was incubated with Ace2-expressing cells for 48 hours. HT1080_{Ace2}
453 cl. 14 cells (27) were used for plasma-derived IgG/IgA and 293T_{Ace2} cells (11) for monoclonal antibodies. Following
454 incubation, cells were washed twice with PBS and lysed with Luciferase Cell Culture Lysis 5x reagent (Promega).
455 Nanoluc Luciferase activity in lysates was measured using the Nano-Glo Luciferase Assay System (Promega) with a
456 GloMax Natigator Microplate Luminometer (Promega). Relative luminescence units obtained were normalized to
457 those derived from cells infected with SARS-CoV-2 pseudotyped virus in the absence of plasma-derived or
458 monoclonal antibodies. The half-maximal and 90% inhibitory concentrations for purified plasma IgG or IgA or
459 monoclonal antibodies (IC₅₀ and IC₉₀) were determined using 4-parameter nonlinear regression (GraphPad Prism).

460

461

462 **Antibody sequencing, cloning and expression**

463 Single B cells were isolated from COV21, COV47 and COV96 patients as previously described(11). Briefly, RNA
464 from single cells was reverse-transcribed (SuperScript III Reverse Transcriptase, Invitrogen, 18080-044) using
465 random primers (Invitrogen, 48190011) and followed by nested PCR amplifications and sequencing using the
466 primers for heavy chain that are listed in (table S7) and primers light chains from (39). Sequence analysis was
467 performed with MacVector. Antibody cloning from PCR products was performed as previously described by
468 sequencing and ligation-independent cloning into antibody expression vectors (Ig γ 1-, IG κ -, IG λ -, Ig α 1 and Ig α 2) as
469 detailed in (40). The Ig α 1 and Ig α 2 vectors were from (Invivogen, pfusess-hcha1 for IgA1 and pfusess-hcha2m1 for
470 IgA2). J chain plasmid was a gift from Susan Zolla-Pazner. Recombinant monoclonal antibodies were produced and
471 purified as previously described (39, 41). Briefly, monoclonal antibodies were produced by transient co-transfection
472 of 293-F cells with human heavy chain and light chain antibody expression plasmids using polyethylenimine (PEI)
473 (Sigma-Aldrich, catalog #408727). Seven days after transfection, supernatants were harvested, clarified by
474 centrifugation and subsequently incubated with Peptide M(Invivogen)/Protein G-coupled sepharose beads
475 (Invivogen, catalog# gel-pdm-5; GE healthcare, 17-0618-05) overnight at 4°C. For dimers, antibodies were
476 produced by transient transfection of Expi293F cells with heavy chain, light chain and J chain expression plasmids
477 at a 1:1:1 ratio. After five days, antibodies were harvested, filtered, incubated with Peptide M overnight and eluted.
478

479 **Separation of Dimeric IgA from its Monomeric Form by Size Exclusion Chromatography**

480 A Pre-packed HiLoad™ 16/60 Superdex™ 200 pg (Cytiva, catalog #28989335) on the NGC™ Quest 10 Plus
481 Chromatography System by Bio-Rad was calibrated at room temperature using the HMW Gel Filtration Calibration
482 Kit (Cytiva, catalog #28403842) and IgG. After equilibration of the column with PBS, each concentrated IgA
483 preparation was applied onto the column using a 1 ml-loop at a flow rate of 0.5 ml/min. Dimers of IgA1 or IgA2
484 were separated from monomers upon an isocratic elution with 70 ml of PBS. The fractions were pooled,
485 concentrated and evaluated by SDS-PAGE using 4 –12% Bis–Tris Novex gels (GenScript catalog #M00652) under
486 reducing and non-reducing conditions followed by a Coomassie blue staining (Expedeon, catalog #ISB1L).
487

488 **Microneutralization assay with authentic SARS-CoV-2.**

489 Production of SARS-CoV-2 virus was performed as previously described (11). This assay was performed as
490 described previously (11, 42). VeroE6 cells were seeded at 1×10^4 cells/well into 96-well plates on the day before
491 infection. IgA monomers and dimers were serially diluted (4-fold) in BA-1, consisting of medium 199 (Lonza, Inc.)
492 supplemented with 1% bovine serum albumin (BSA) and 1x penicillin/streptomycin. The diluted samples were
493 mixed with a constant amount of SARS-CoV-2 and incubated for 1hr at 37°C. The antibody-virus-mix was then
494 directly applied to VeroE6 cells (MOI of ~0.1 PFU/cell; n=3) and incubated for 22h at 37°C. Cells were
495 subsequently fixed by adding an equal volume of 7% formaldehyde to the wells, followed by permeabilization with
496 0.1% Triton X-100 for 10 min. After extensive washing, cells were incubated for 1hr at 37°C with blocking solution
497 of 5% goat serum in PBS (catalog no. 005-000-121; Jackson ImmunoResearch). A rabbit polyclonal anti-SARS-
498 CoV-2 nucleocapsid antibody (catalog no. GTX135357; GeneTex) was added to the cells at 1:1,000 dilution in
499 blocking solution and incubated at 4 °C overnight. Goat anti-rabbit AlexaFluor 594 (catalog no. A-11012; Life
500 Technologies) was used as a secondary antibody at a dilution of 1:2,000. Nuclei were stained with Hoechst 33342
501 (catalog no. 62249; Thermo Scientific) at a 1:1,000 dilution. Images were acquired with a fluorescence microscope
502 and analyzed using ImageXpress Micro XLS (Molecular Devices, Sunnyvale, CA). All experiments involving
503 SARS-CoV-2 were performed in a biosafety level 3 laboratory.

504

505 **Biolayer interferometry**

506 BLI assays were performed on the Octet Red instrument (ForteBio) at 30 °C with shaking at 1,000 r.p.m. Epitope
507 binding assays were performed with protein A biosensor (ForteBio 18-5010), following the manufacturer's protocol
508 "classical sandwich assay". (1) Sensor check: sensors immersed 30 sec in buffer alone (buffer ForteBio 18-1105).
509 (2) Capture 1st Ab: sensors immersed 10 min with Ab1 at 40 µg/mL. (3) Baseline: sensors immersed 30 sec in
510 buffer alone. (4) Blocking: sensors immersed 5 min with IgG isotype control at 50 µg/mL. (6) Antigen association:
511 sensors immersed 5 min with RBD at 100 µg/mL. (7) Baseline: sensors immersed 30 sec in buffer alone. (8)
512 Association Ab2: sensors immersed 5 min with Ab2 at 40 µg/mL. Curve fitting was performed using the Fortebio
513 Octet Data analysis software (ForteBio).

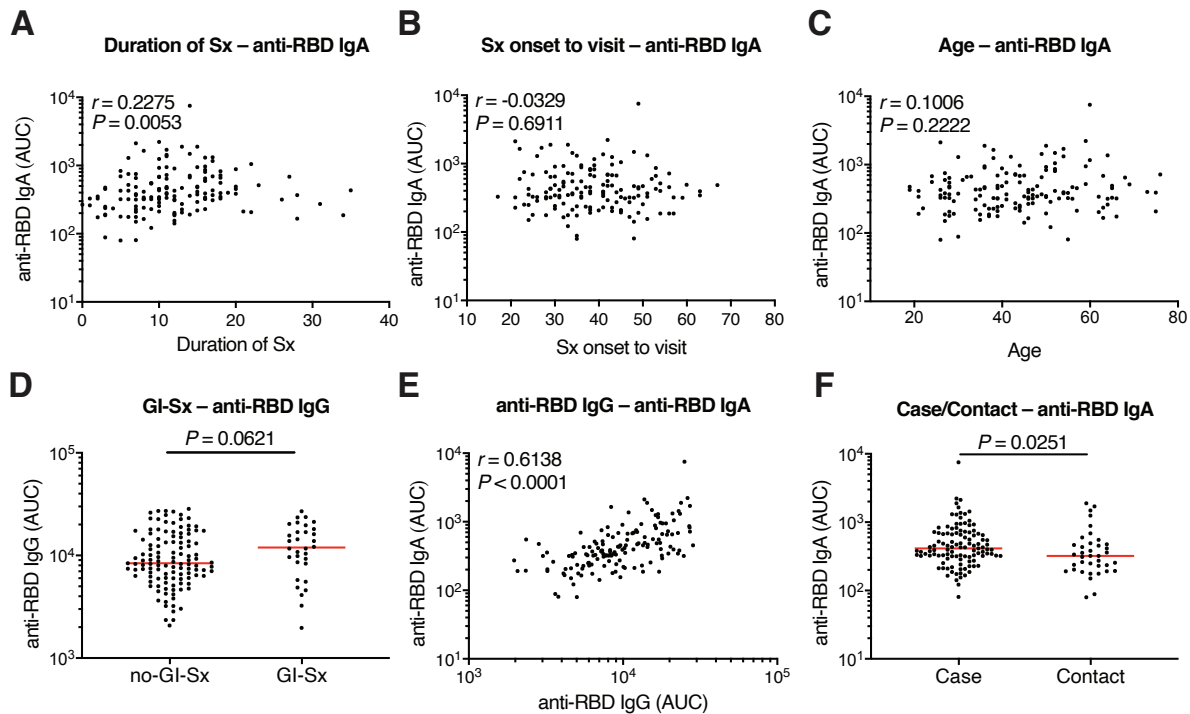
514

515 **Computational analyses of antibody sequences**

516 Antibody sequences were trimmed based on quality and annotated using Igblastn v1.14.0[ref] with IMGT domain
517 delineation system. Annotation was performed systematically using Change-O toolkit v.0.4.5(43). Heavy and light
518 chains derived from the same cell were paired, and clonotypes were assigned based on their V and J genes using in-
519 house R and Perl scripts (Fig. 3 A and B). All scripts and the data used to process antibody sequences are publicly
520 available on GitHub (<https://github.com/stratust/igpipeline>). Nucleotide somatic hypermutation and CDR3 length
521 were determined using in-house R and Perl scripts. For somatic hypermutations, IGHV and IGLV nucleotide
522 sequences were aligned against their closest germlines using Igblastn and the number of differences were considered
523 nucleotide mutations. The average mutations for V genes was calculated by dividing the sum of all nucleotide
524 mutations across all patients by the number of sequences used for the analysis. Hydrophobicity distribution
525 comparisons were calculated as described in (11) (Fig. S5). The frequency distributions of human V genes in anti-
526 SARS-CoV-2 antibodies from this study was compared to 131,284,220 IgH and IgL sequences generated by (44)
527 and downloaded from cAb-Rep (45), a database of human shared BCR clonotypes available at [https://cab-](https://cab-rep.c2b2.columbia.edu/)
528 [rep.c2b2.columbia.edu/](https://cab-rep.c2b2.columbia.edu/). Based on the 81 distinct V genes that make up the 1455 analyzed sequences from Ig
529 repertoire of the three patients present in this study, we selected the IgH and IgL sequences from the database that
530 are partially coded by the same V genes and counted them according to the constant region. The frequencies shown
531 in (Fig. S6) are relative to the source and isotype analyzed. We used the two-sided binomial test to check whether
532 the number of sequences belonging to a specific IgHV or IGLV gene in the repertoire is different according to the
533 frequency of the same IgV gene in the database. Adjusted p-values were calculated using the false discovery rate
534 (FDR) correction. Significant differences are denoted with stars.

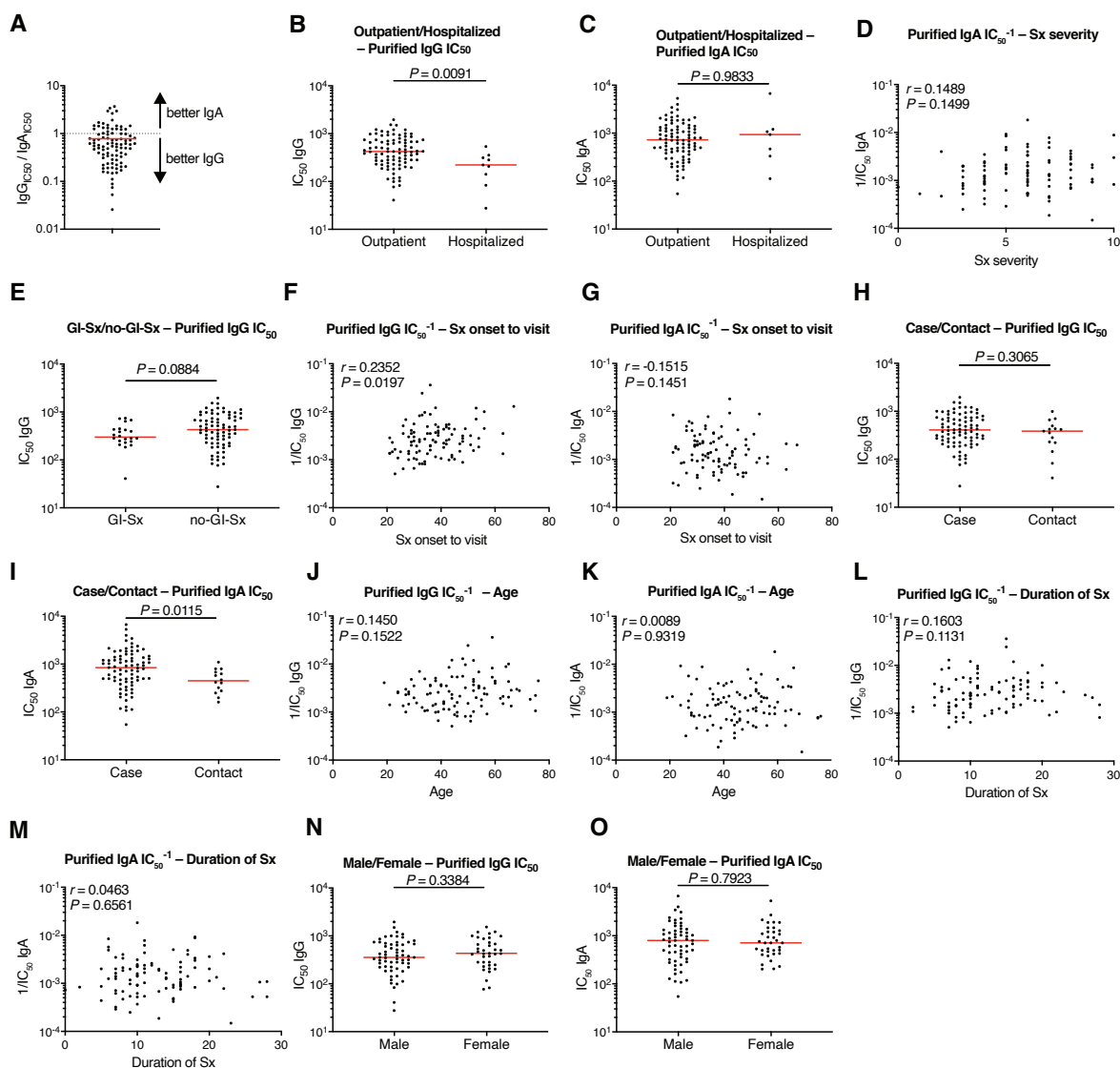
535

536



537

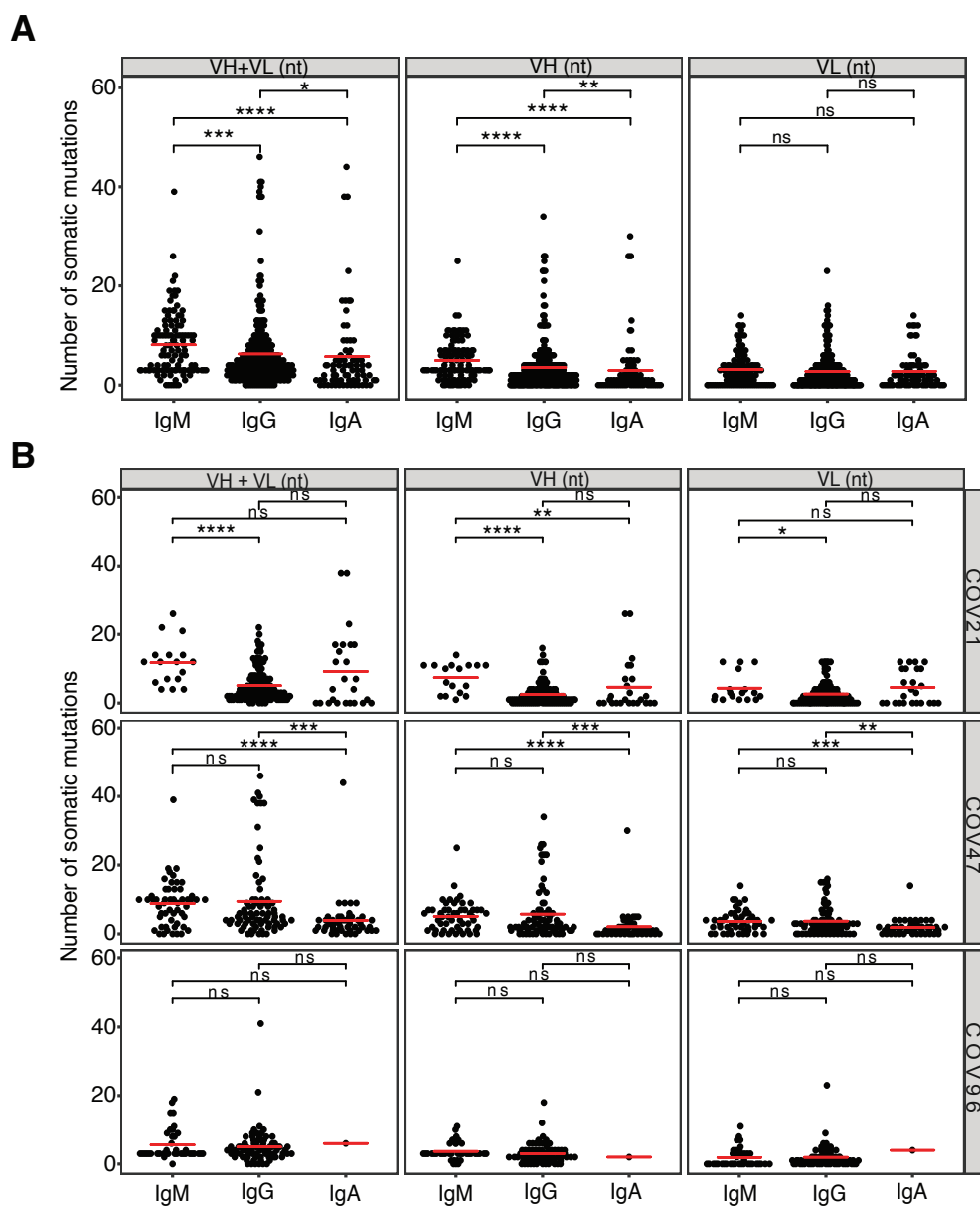
538 **Fig. S1 Clinical correlates of plasma IgA antibody titers** (A) Duration of Symptom (Sx) in days (X axis) plotted
539 against normalized AUC for plasma IgA binding to RBD (Y axis). $r = 0.2275$, $P = 0.0053$. (B) Sx onset to time of
540 sample collection in days plotted against normalized AUC for plasma IgA anti-RBD. $r = -0.0329$ and $P = 0.6911$.
541 (C) Age plotted against normalized AUC for plasma IgA anti-RBD. $r = 0.1006$, $P = 0.2222$. (D) Normalized AUC
542 of plasma anti-RBD IgG ELISA for patients with gastrointestinal (GI) symptoms (n=32) and without GI symptoms
543 (n=117); $P = 0.0621$. (E) Normalized AUC of plasma anti-RBD IgG ELISA plotted against normalized AUC for
544 plasma IgA anti-RBD. $r = 0.6138$, $P < 0.0001$. (F) Normalized AUC of plasma anti-RBD IgA ELISA for all cases (n
545 = 111) and contacts (n = 38) in the cohort; $P = 0.0251$. For (A-C, E) the correlations were analyzed by two-tailed
546 Spearman's tests; For (D and F), Horizontal bars indicate median values. Statistical significance was determined
547 using two-tailed Mann-Whitney U-tests.



548

549 **Fig. S2 Clinical correlates of plasma IgA/IgG neutralization** (A) Ratio of pseudovirus neutralization IC₅₀ values
 550 of purified IgG to IgA (n=95). (B, C) Purified plasma IgG (B) and IgA(C) pseudovirus neutralizing IC₅₀ values for
 551 all outpatient (n = 90) and hospitalized (n = 9) participants in the cohort. (Fig. S2B, $P = 0.0091$) and (Fig. S2C, $P =$
 552 0.9833). (D) Purified plasma IgA $1/IC_{50}$ values plotted against symptom severity. $r = 0.1489$, $P=0.1499$. (E) Purified
 553 plasma IgG IC₅₀ values for patients with GI symptoms (n=22) and without GI symptoms (n=77); $p=0.0884$. (F, G)
 554 Sx onset to time of sample collection in days plotted against purified plasma IgG (F) and IgA(G) pseudovirus
 555 neutralization $1/IC_{50}$ values. (Fig. S2F, $r = 0.2352$, $P = 0.0197$) and (Fig. S2G, $r = -0.1515$, $P = 0.1451$). (H, I)
 556 Purified plasma IgG (H) and IgA(I) pseudovirus neutralization IC₅₀ values for all cases (n = 84) and contacts (n =
 557 15) in the cohort. (Fig. S2H, $P = 0.3065$) and (Fig. S2I, $P = 0.0115$). (J, K) Age plotted against purified plasma IgG

558 (J) and IgA(K) pseudovirus neutralization $1/IC_{50}$ values. (Fig. S2J, $r = 0.1450$, $P = 0.1522$) and (Fig. S2K, $r =$
559 0.0089 , $P = 0.9319$). (L, M) Duration of Symptom (Sx) in days (X axis) plotted against purified plasma IgG (L) and
560 IgA(M) pseudovirus neutralization $1/IC_{50}$ values. (Fig. S2L, $r = 0.1603$, $P = 0.1131$) and (Fig. S2M, $r = 0.0463$, $P =$
561 0.6561). (N, O) Purified plasma IgG (N) and IgA(O) pseudovirus neutralization IC_{50} values for males ($n=61$) and
562 females ($n=38$). (Fig. S2N, $P=0.3384$) and (Fig.S2O, $P=0.7923$). For (A), horizontal bars indicate mean value. For
563 (B, C, E, H, I, N, O), horizontal bars indicate median values. Statistical significance was determined using two-tailed
564 Mann–Whitney U-tests; For (D, F, G, J-M), the correlations were analyzed by two-tailed Spearman’s tests.
565



566

567

Fig. S3 Analysis of antibody somatic hypermutation

568

(A) The number of somatic nucleotide mutations (Y axis) at the IGVH and IGVL for IgM, IgG and IgA antibodies

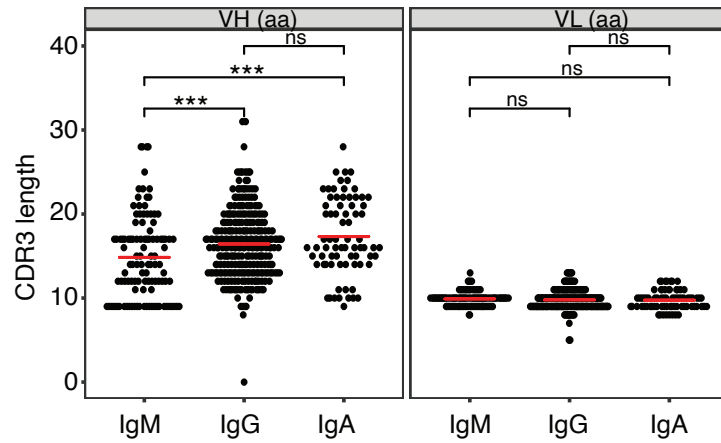
569

(X axis), the horizontal bars indicate the mean. The number of antibody sequences was evaluated for both IGVH and

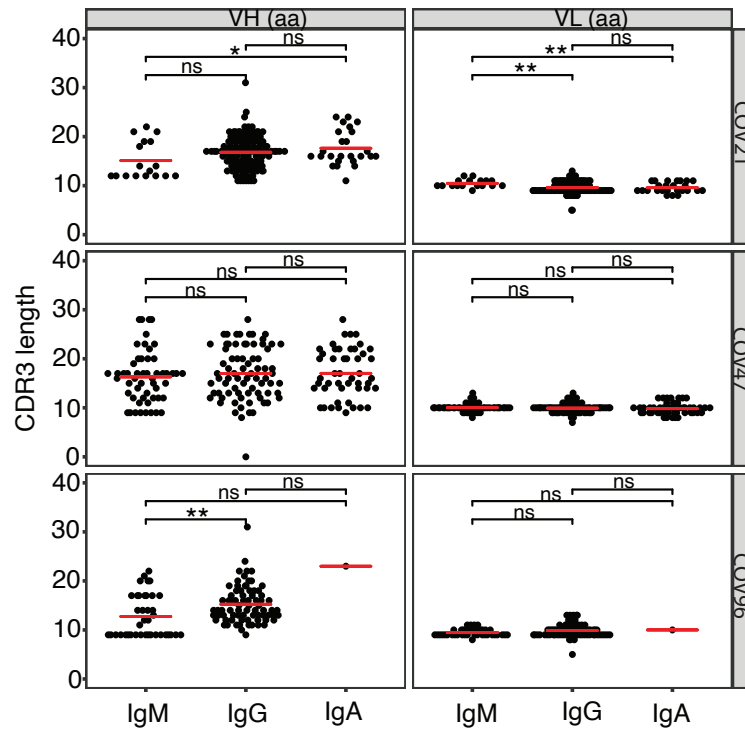
570

IGVL. (n=455). (B) Same as (A) but for each individual.

A



B



571

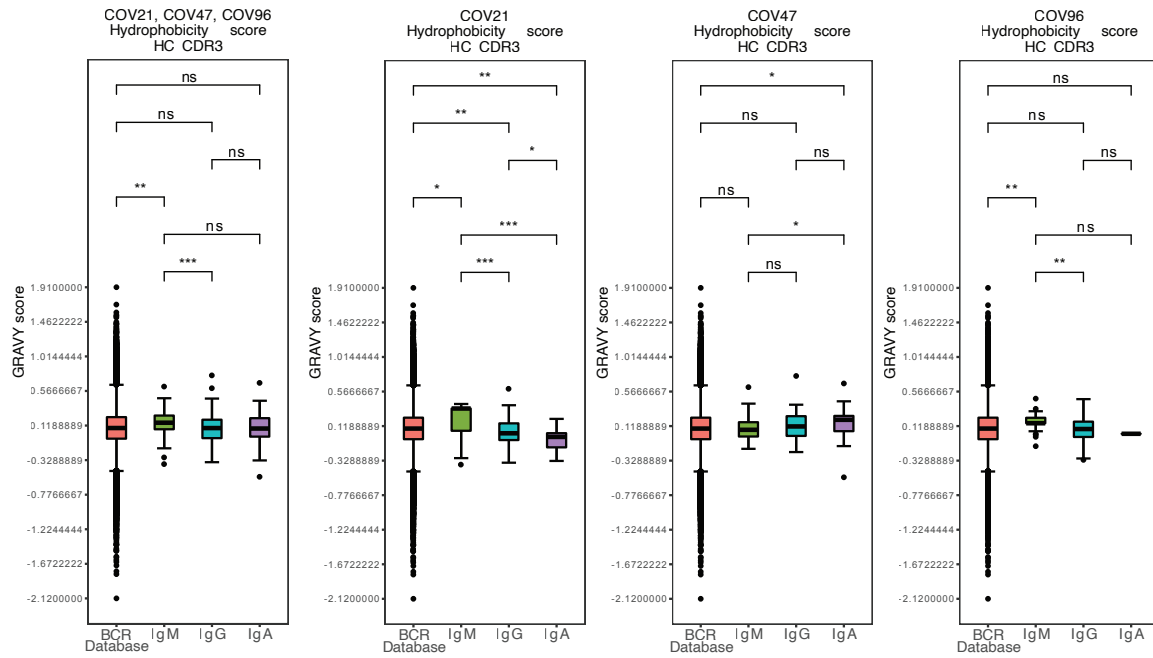
572 **Fig. S4 Analysis of antibody CDR3 length**

573 (A) IGHV and IGLV CDR3s length (Y axis) for IgM, IgG and IgA (X axis). (B) Same as (A) but for each

574 individual. The horizontal bars indicate the mean.

575

576

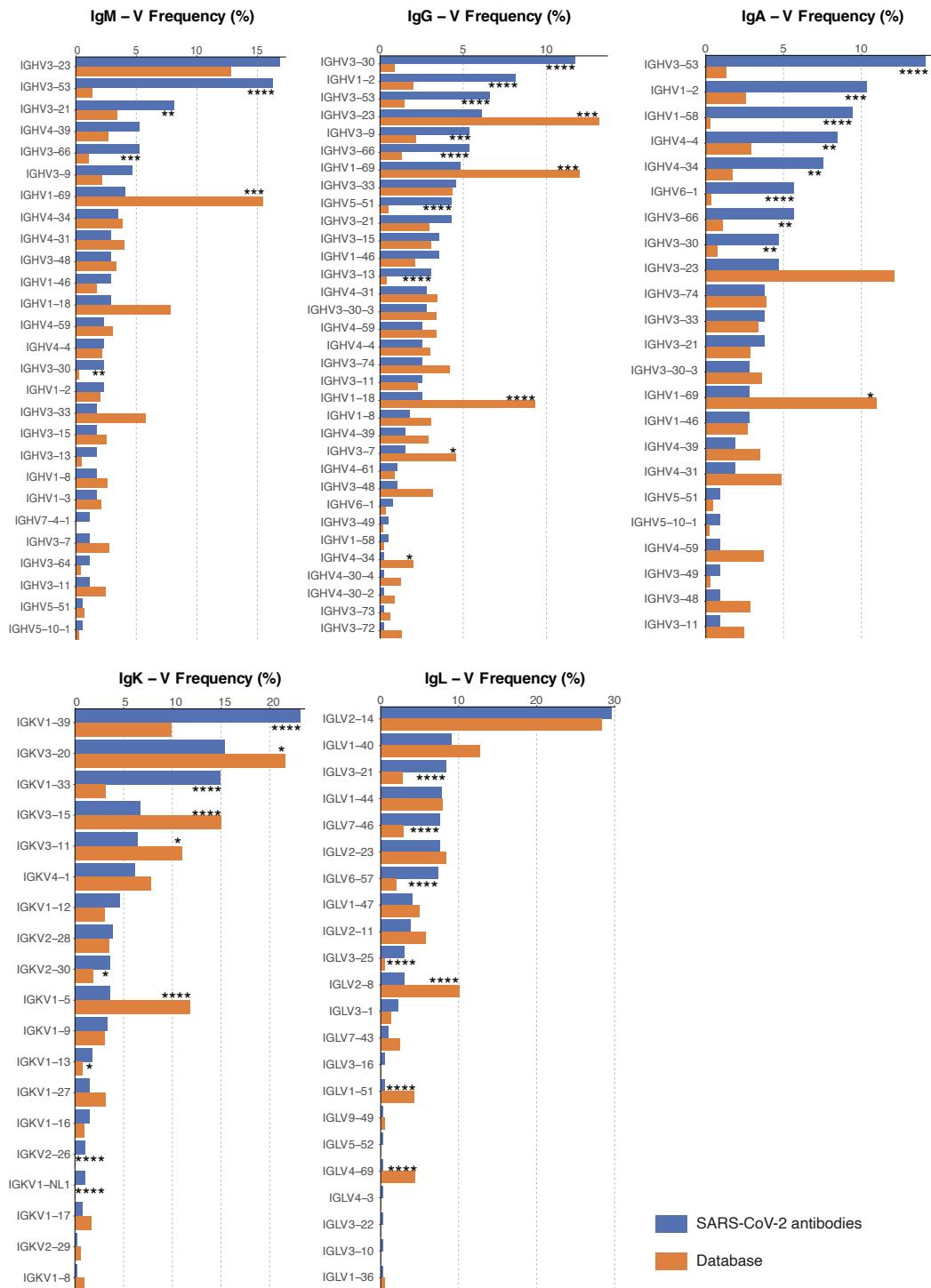


577

578 Fig. S5 Analysis of antibody CDR3 hydrophobicity

579 Distribution of the hydrophobicity GRAVY scores at the IGH CDR3 in antibody sequences from this study
580 compared to a public database (see Methods for statistical analysis). The box limits are at the lower and upper
581 quartiles, the center line indicates the median, the whiskers are 1.5x interquartile range and the dots represent
582 outliers.

583



584

585 **Fig. S6 Frequency distributions of human V genes.**

586 Comparison of the frequency distributions of human V genes for heavy chain (IgM, IgG and IgA) and light chains

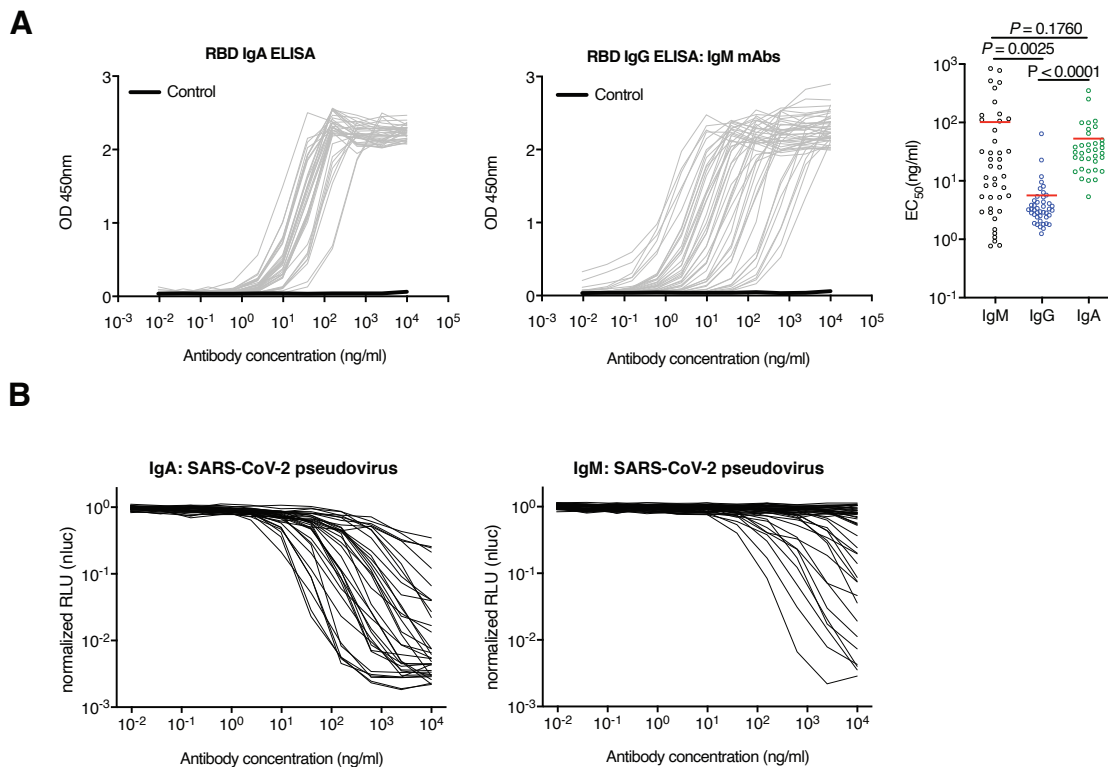
587 of anti-SARS-CoV-2 antibodies from this study and from a database of shared clonotypes of human B cell receptor

588 generated by Cinque Soto et al. (44). Statistical significance was determined using the two-sided binomial test.

589 Significant differences are denoted with stars.

590

591

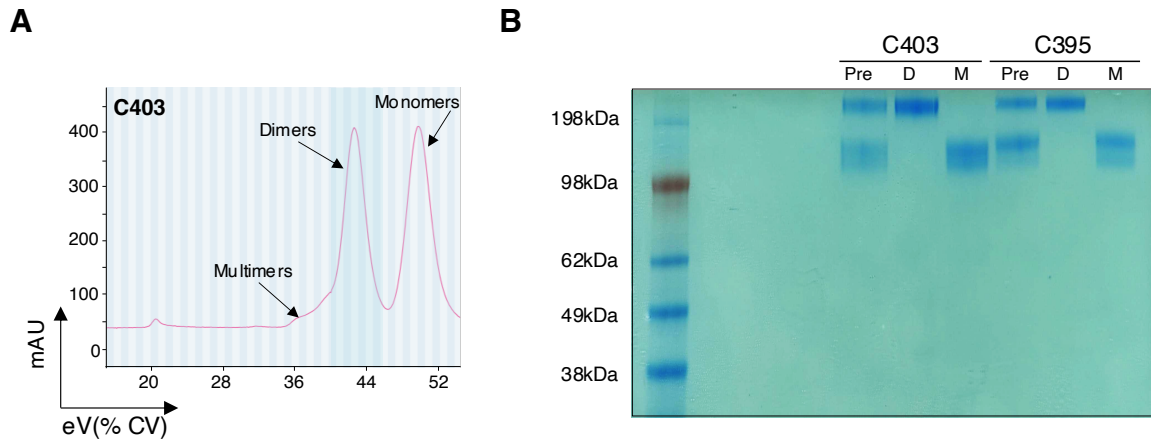


592

593 **Fig. S7 Binding and neutralizing activity of anti-SARS-CoV-2 RBD IgA and IgM monomers.**

594 (A) Binding profiles of 35 IgA and 46 IgM monoclonals against RBD. Comparisons of IgM, published IgG (11) and
595 IgA EC_{50} values shown as in right panel. Red lines indicate mean value. (B) The normalized relative luminescence
596 values for cell lysates of 293T_{ACE2} cells 48 h after infection with SARS-CoV-2 pseudovirus in the presence of
597 increasing concentrations of monoclonal IgA and IgM antibodies. Statistical analysis was performed using the
598 student's *t* test.

599



600

601

602

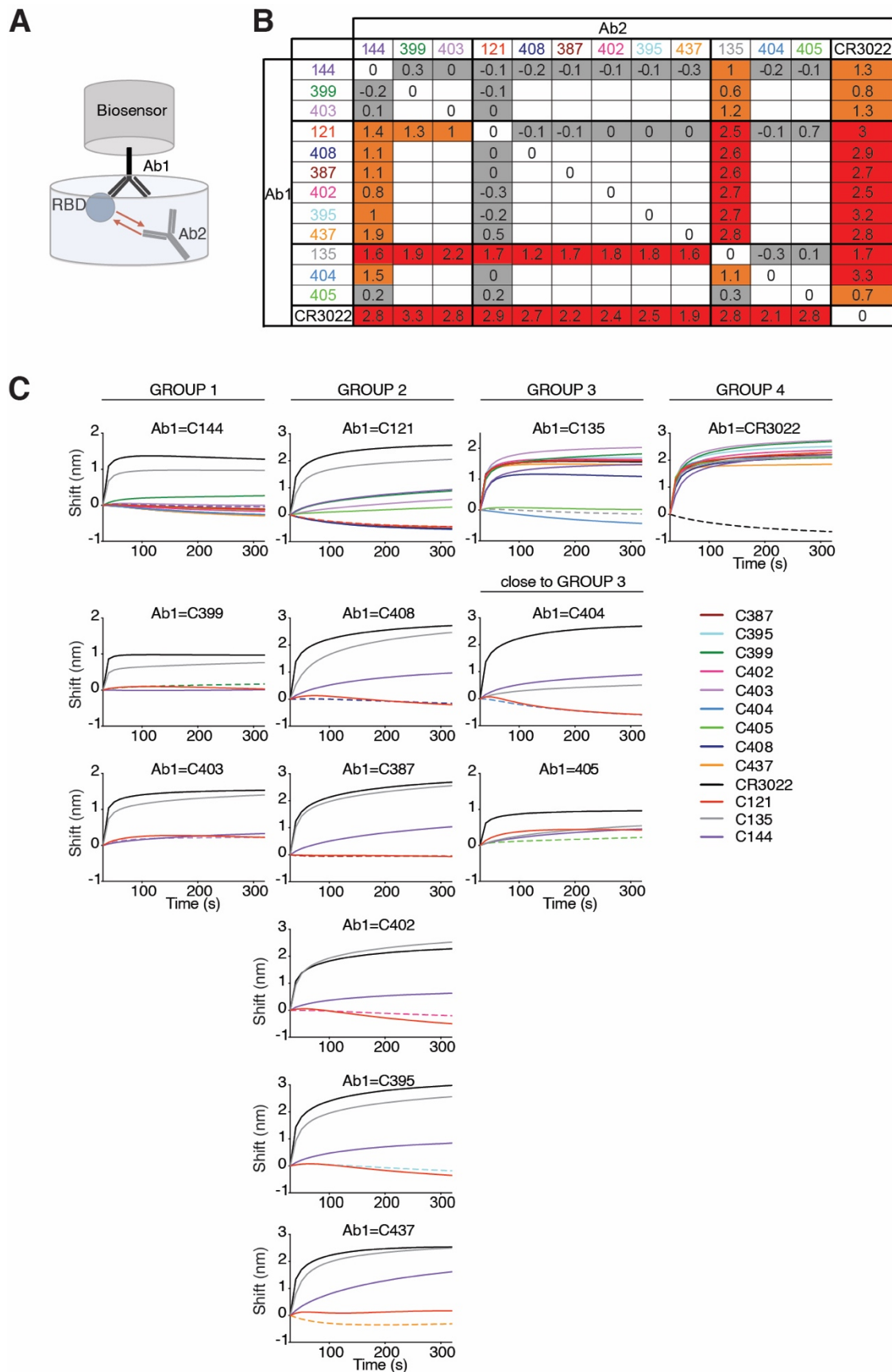
603

604

605

606

Fig. S8 Purification of Dimeric IgA by Size Exclusion Chromatography. (A) Monomers and dimers of IgA1 or IgA2 were separated using a Superdex 200 (Cytiva) with PBS at a flow rate of 0.5 ml/min. Representative example: C403. The X axis is elution volume (eV) as a percent of Column volume. The Y axis is absorption at 280nm (mAU). (B) Coomassie Blue stained non-reducing SDS-PAGE gel of pre-separation antibody mixture (Pre), isolated dimers (D) and monomers (M).



608 **Fig. S9 Biolayer interferometry experiment.** (A) Diagrammatic representation of biolayer interferometry
609 experiment. (B) The table displays the shift in nanometers after second antibody (Ab2) binding to the antigen in the
610 presence of the first antibody (Ab1). Values are normalized by the subtraction of the autologous antibody control.
611 (C) Second antibody (Ab2) binding to preformed first antibody (Ab1)–RBD complexes. Dotted line denotes when
612 Ab1 and Ab2 are the same, and Ab2 is according to the colour-coding in Fig. 4B (right panel).
613

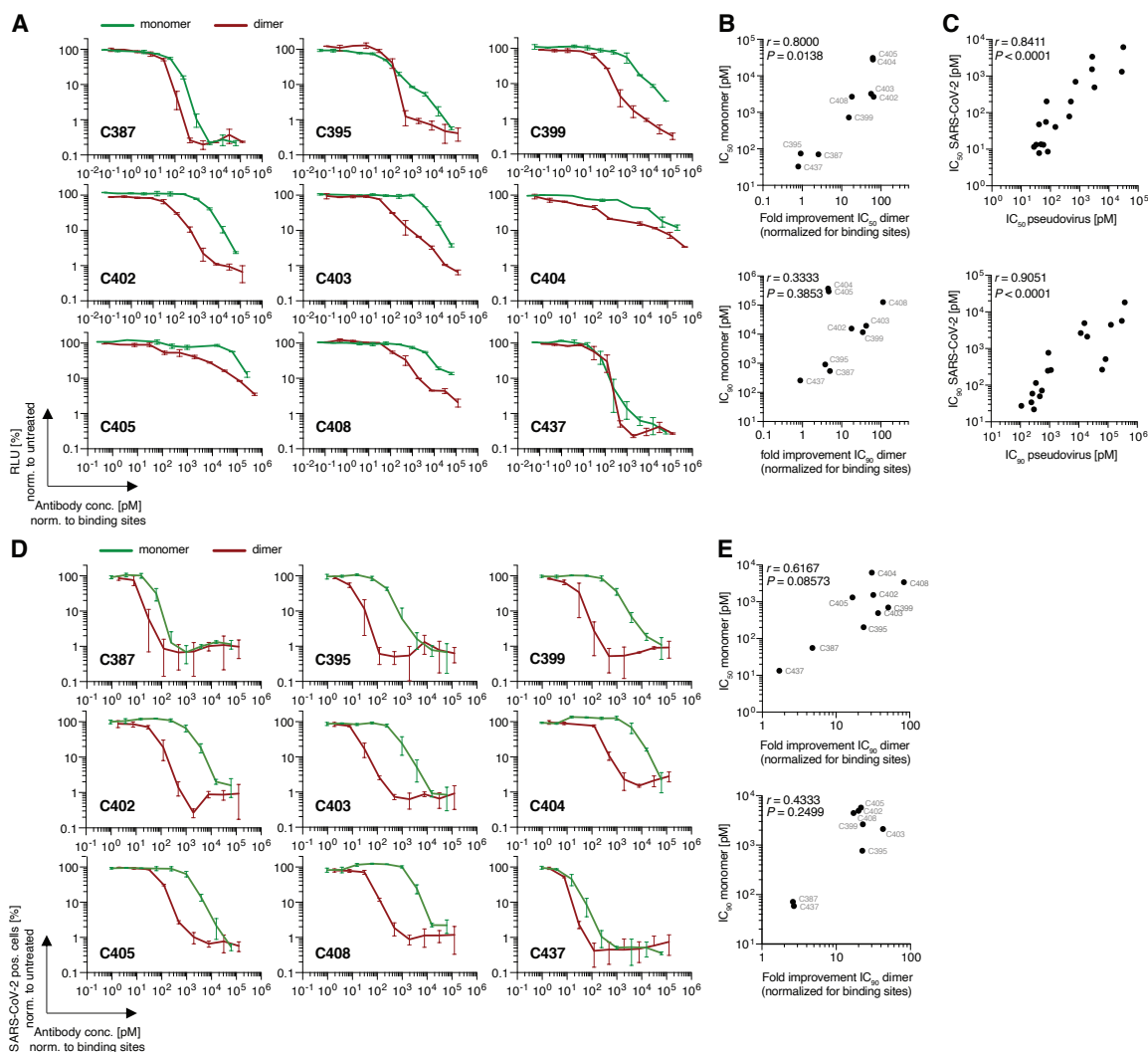


Fig. S10 Neutralizing activity of monoclonal monomeric and dimeric IgAs

(A) The normalized relative luminescence values for cell lysates of 293T_{ACE2} cells 48 h after infection with SARS-CoV-2 pseudovirus in the presence of increasing concentrations of monoclonal antibodies C387, C395, C399, C402, C403, C404, C405, C408, C437 in their monomeric (green curves) and dimeric (red curves) form. (B) Fold improvement of the IC₅₀ (upper panel) and IC₉₀ (lower panel) values of dimeric IgA to monomeric IgA (X axis) plotted against IC₅₀ ($r = 0.8000$, $P = 0.0138$), IC₉₀ ($r = 0.3333$, $P = 0.3853$) values of monomeric IgAs. (C) IC₅₀ (upper panel) and IC₉₀ (lower panel) values of dimeric and monomeric IgAs determined by pseudovirus neutralization assay (x axis) plotted against IC₅₀ ($r = 0.8411$, $P < 0.0001$) and IC₉₀ ($r = 0.9051$, $P < 0.0001$) values

625 determined by authentic SARS-CoV-2 neutralization assay (y axis). (D) SARS-CoV-2 neutralization assay. The
 626 normalized percentage of SARS-CoV-2 positive VeroE6 cells 48 h after infection with SARS-CoV-2 authentic virus
 627 in the presence of increasing concentrations of abovementioned antibodies in their dimeric and monomeric form. (E)
 628 Fold improvement of the IC₅₀ (upper panel) and IC₉₀ (lower panel) values of dimeric IgA to monomeric IgA (X axis)
 629 plotted against IC₅₀ ($r = 0.6167$, $P = 0.08573$), IC₉₀ ($r = 0.4333$, $P = 0.2499$) values of monomeric IgAs. Correlations
 630 were analyzed by two-tailed Spearman's tests.

631

632

633

634 **Table S1. Sequences of anti-SARS-CoV-2 antibodies**

635 Auxiliary Supplementary Material.

636

637 **Table S2. Sequences of antibodies from isotype shared clones**

638 Auxiliary Supplementary Material.

639

640 **Table S3. Inhibitory concentrations of monoclonal antibodies from isotype shared clones**

Patient ID	IgM	IC50(ng/ml)	IC90(ng/ml)	IgG	IC50(ng/ml)*	IC90(ng/ml)*	IgA	IC50(ng/ml)	IC90(ng/ml)
COV21	-			CG002	8.88	37.61	CA386	5.76	123.33
	-			CG005	60.49	205.20	CA387	9.68	129.87
COV47	-			CG144	6.91	29.66	CA394	13.06	371.86
	CM169	UD	UD	CG148	>1000	>1000	-		
	CM170	5806	37082	CG171	5250	17156	CA457	1721.6	298325.6
	-			CG379	126.98	2368.18	CA403	23.88	126.05
	CM381	UD	UD	CG160	>1000	>1000	-		
	CM349	844.59	26446.73	CG380	2.94	35.96	-		
	CM311	126.85	846.13	CG151	31.79	>1000	CA390	417.42	46597.44
COV96	CM194	UD	UD	CG382	42.92	122.33	-		
	CM365	1226.09	8268.46	CG202	>1000	>1000	-		

UD=Undetectable

*(Robbiani et al. 2020)

641

642 **Table S4. Sequences of cloned recombinant antibodies**

643 Auxiliary Supplementary Material.

644

645 **Table S5. Effective and inhibitory concentrations of monoclonal antibodies**

646 Auxiliary Supplementary Material.

647

648 **Table S6. Inhibitory concentrations of monoclonal IgA monomers and dimers**

Table S6. Inhibitory concentrations of monoclonal IgA monomers and dimers

Antibody ID	SARS-CoV-2 pseudovirus				SARS-CoV-2			
	IC50 (pM)		IC90 (pM)		IC50 (pM)		IC90 (pM)	
	monomer	dimer	monomer	dimer	monomer	dimer	monomer	dimer
C387	70.68	27.46	543.91	108.06	55.74	11.64	71.46	27.37
C395	74.15	81.64	909.67	239.03	203.72	8.59	769.49	34.10
C399	722.84	47.48	11692.05	339.46	700.38	13.67	2636.98	114.74
C402	2652.52	40.86	15603.86	874.99	1536.24	47.90	4939.53	247.79
C403	3222.29	57.62	19499.80	461.45	491.11	13.18	2115.67	49.85
C404	31112.25	502.11	371134.20	82318.65	6182.08	201.78	18271.60	514.05
C405	27801.09	444.36	294918.48	62867.98	1312.88	78.57	5725.29	266.04
C408	2691.09	147.89	126130.74	1114.44	3392.62	40.51	4458.13	259.84
C437	32.67	41.18	258.08	292.35	13.32	7.84	58.85	21.82

IC50/90 values for dimers were adjusted for number of binding sites

649

650 **Table S7. Primers**

651 Auxiliary Supplementary Material.

652

653

654

655

656